Engineering the shape and structure of materials by fractal cut

Yigil Cho[a], Joong-Ho Shin[a], Avelino Costa[a], Tae Ann Kim[b], Valentin Kunin[c], Ju Li[d], Su Yeon Lee[e], Shu Yang[e], Heung Nam Han[f], In-Suk Choi[a,1], and David J. Srolovitz[e,g]

[a]High Temperature Energy Materials Research Center and [b]Photo-Electronic Hybrids Research Center, Korea Institute of Science and Technology, Seoul 136-791, South Korea; [c]Graduate Group in Applied Mathematics and Computational Science and Departments of [e]Materials Science and Engineering and [g]Mechanical Engineering and Applied Mechanics, University of Pennsylvania, Philadelphia, PA 19104; [d]Departments of Nuclear Science and Engineering, and Materials Science and Engineering, Massachusetts Institute of Technology, Cambridge, MA 02139; and [f]Department of Materials Science and Engineering, Research Institute of Advanced Materials, Seoul National University, Seoul 151-744, South Korea

Edited by John W. Hutchinson, Harvard University, Cambridge, MA, and approved October 30, 2014 (received for review September 15, 2014)

In this paper we discuss the transformation of a sheet of material into a wide range of desired shapes and patterns by introducing a set of simple cuts in a multilevel hierarchy with different motifs. Each choice of hierarchical cut motif and cut level allows the material to expand into a unique structure with a unique set of properties. We can reverse-engineer the desired expanded geometries to find the requisite cut pattern to produce it without changing the physical properties of the initial material. The concept was experimentally realized and applied to create an electrode that expands to >800% the original area with only very minor stretching of the underlying material. The generality of our approach greatly expands the design space for materials so that they can be tuned for diverse applications.

expandability | patterning | flexibility | differentiation | deformability

The physical properties of materials are largely determined by structure: atomic/molecular structure, phase distribution, internal defects, nano/microstructure, sample geometry, and electronic structure. Among these, engineering the geometry of the sample can provide a direct, intuitive, and often material-independent approach to achieve a predetermined set of properties. Metamaterials are fabricated based on geometric concepts (1–16). In two dimensions, periodic geometries have been adopted to tune the mechanical properties of membranes (3–8, 10, 12–14). From simple shapes such as circles (3), triangles (6, 7, 12, 13), and quadralaterals (4, 5, 14) to more complex shapes (8, 10), a broad range of mechanical behavior has been observed, including pattern transformation, negative Poisson's ratio (auxetic), elastic response, and isostaticity. *Origami* and *kirigami*, the arts of paper folding and paper cutting, create beautiful patterns and shapes that have attracted the attention of scientists to two-dimensional materials (e.g., graphene, polymer films, and so on) (11, 17–19). However, application of conventional origami and kirigami approaches to achieve desired material response requires complex cutting and/or folding patterns that are often incompatible with engineering materials. In this paper we propose an advanced approach to the design of two-dimensional structures that can achieve a wide range of desirable programmed shapes and mechanical properties.

This study starts from the question, Can we design two-dimensional structures that can be formed by simply cutting a sheet, that can morph into a specific shape? In nature, many biological and natural system (20) can be found that use hierarchical structure to produce different properties and/or shapes. One such example is a stem cell. An embryonic, pluripotent stem cell can differentiate into any type of cell in the body (21). By recursively dividing, the stem cell can transform into particular cell types or remain unspecialized with the potential to transform. For a material, one aspect of recursive hierarchical geometry was recently discussed for applications in flexible electronics (22). Here, by analogy to the stem cell, we demonstrate that starting from a simple sheet of material (the pluripotent state) it is possible to apply different hierarchical cut patterns (differentiation) to achieve a wide range of macroscopic (unipotent) shapes. In particular, we focus on "fractal cut" patterns that allow for precise control of differentiated material structures. Our goal is to broaden the design space for engineered materials and systems for a wide range of applications, such as flexible/stretchable devices, photonic materials, and bioscaffolds. We illustrate the concept through numerical simulation, theory, and experimental realization.

Basic Principle: Rotating Units

For simplicity, we focus on a base material in the form of a flat, flexible sheet and subject it to a prescribed cut pattern. The essence of the design is that cuts divide the material into rotating units, depending on the cut pattern (4, 5), as exemplified in Fig. 1*A*. The units (e.g., squares or triangles) between cuts are effectively rigid and the connections between these units behave as (nearly) free rotational hinges, such that the deformation of the structure (e.g., biaxial or uniaxial stretching) occurs primarily through rotation of the units, rather than by significant deformation of the units themselves. The final material morphology, determined by the cut pattern, is determined through moment equilibrium (23). There is a maximum stretch ratio (strain) that can be achieved by rotation for any specific cut pattern beyond which the units themselves will deform; this latter stage of deformation is conventional and is not of interest here.

Significance

Most materials can be stretched to a small degree, depending on their elastic limits and failure properties. For most materials the maximum elastic dilatation is very small, implying that the macroscopic shapes to which an elastic body can be deformed is severely limited. The present work addresses the simple modification of any material via hierarchical cut patterns to allow for extremely large strains and shape changes and a large range of macroscopic shapes. This is an important step in the development of shape-programmable materials. We provide the mathematical foundation, simulation results, and experimental demonstrations of the concept of fractal cut. This approach effectively broadens the design space for engineered materials for applications ranging from flexible/stretchable devices and photonic materials to bioscaffolds.

Author contributions: Y.C. and I.-S.C. conceived the concept of the fractal cut and designed research; Y.C., J.-H.S., A.C., T.A.K., S.Y.L., S.Y., and I.-S.C. contributed experimental realization; V.K. and D.J.S. contributed the geometric model; Y.C., H.N.H., and I.-S.C. performed finite element simulations; Y.C., V.K., J.L., I.-S.C., and D.J.S. analyzed data; and Y.C., S.Y., I.-S.C., and D.J.S. wrote the paper.

Conflict of interest statement: Y.C. and I.-S.C. have filed a patent application relating to expandable electrodes based on the fractal cut pattern.

This article is a PNAS Direct Submission.

[1]To whom correspondence should be addressed. Email: insukchoi@kist.re.kr.

This article contains supporting information online at www.pnas.org/lookup/suppl/doi:10.1073/pnas.1417276111/-/DCSupplemental.

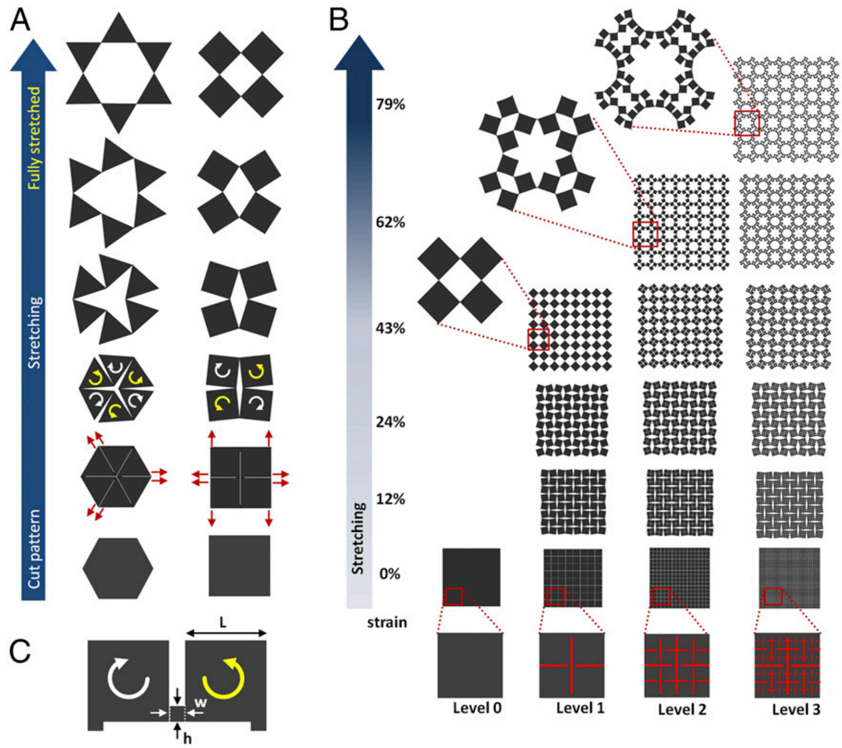

Fig. 1. Basic principles of the cut design. (*A*) Cuts separate the material into rotating units, with connectivity dependent on the cut pattern (assuming freely rotating point hinges). A hexagon can be divided into six smaller triangles in a pattern that can be repeated to fill space or a square can be divided into four smaller squares. Upon equal-biaxial stretching, each unit rotates clockwise (white arrows) or counterclockwise (yellow arrows), yielding an expansion of the original structure. Expansion continues up to a maximum level by pure unit rotation (minimal strain within the structural units). The structures are fully stretched when moment equilibrium is achieved. If the units are rigid, no further expansion is possible. (*B*) Finite element calculations for finite size hinges (see *C*) in silicone rubber. The cuts can be combined in a multilevel hierarchy. The level-0 structure, which has no embedded cuts, is cut into four smaller squares to make the level- structure. Each such unit is cut into four smaller squares to make a higher-level structure, up to an arbitrary degree/level of hierarchy, *N*. The level-0 structure does not expand because no rotation is possible upon biaxial stressing. In the level-1 structure, each unit can rotate up to 45°. The corresponding lateral strain is 43%. The maximum lateral strains for $n = 2$ and 3 are 62% and 79%, respectively. These finite element results were confirmed by comparison with the geometric model (rigid units and free hinges, as per *A*), the macro/microscopic experiments, and analytical predictions (*Supporting Information*). The pore shape, pore size, and apparent density vary with hierarchy level. (*C*) A schematic of the finite hinge geometry used in the finite element method calculations (*B*) and in the experiments.

Fractal Cut Pattern: Hierarchy

In this paper we discuss two classes of cut patterns: hierarchical and motif alternation. The hierarchical pattern concept is illustrated in Fig. 1*B* for a simple pattern of cuts producing square units. Such square units can be subdivided into smaller squares by repeating the cut pattern within the original square. Although the subdivision can, in principle, go on ad infinitum, creating a true fractal cut pattern (20), we focus on patterns of finite hierarchy degree or level (i.e., the number of times the same cut pattern is reproduced on the units left by the preceding cuts). Increasing the hierarchy level leads to increasingly complex structures and increased expandability. Along with expandability, pore shape, apparent density, and elastic stiffness (assuming the hinges have some resistance to rotation) all vary with the hierarchy level. Examination of Fig. 1*B* shows that the expansion at one level is largely exhausted before the expansion at the next level of the hierarchy operates (cf. level-1, -2 and -3 structures at a biaxial strain of 0.24). (Note: we focus on square units in two dimensions in this discussion, but application to triangular units in two dimensions and cubical units in three dimensions are shown in *Supporting Information*.)

The variables that determine the final structure of the stretched sheet are the rotation angles between rotating units. The number of independent variables increases with increasing level. The level-0 structure, which has no cuts has 0 independent variables (i.e., no degrees of freedom $F_0 = 0$). The level-1 structure has one degree of freedom (one independent angle determining the rotation of all units), $F_1 = 1$. The level-2 and -3 square structures have two and six degrees of freedom, $F_2 = 2$ and $F_3 = 6$, respectively. The number of degrees of freedom grows as $F_N = 4F_{N-1} - 2$ or $F_N = (4^{N-1} + 2)/3$ (for $n > 1$), where N is the hierarchy level. This implies that for any strain smaller than some maximum the structure with free hinges is not fully determined (i.e., there are multiple sets of angles that can lead to exactly the same strain) for any $n \geq 2$ (see *Supporting Information* for a specific example).

Whereas "free hinges" is an idealization, in any real material application the hinges have finite rotational stiffness. Consider the case where the "hinges" consist of the incompletely cut units, as illustrated in Fig. 1*C*. The rotational (bending) stiffness of the hinge is proportional to h^3 (Fig. 1*C*). In any such real case the structure is fully determined at any strain. The maximum stress in the hinge during rotation (bending of the ligament) is proportional to h/w. Hence, appropriate hinge design represents a compromise between hinge failure and hinge stiffness. The geometric parameters describing the hinges in the finite element method calculations and experiments are reported in *Supporting Information*. We note that the design must also be sensitive to the actual choice of materials, in particular the stiffness and the fracture and yield strengths. Although elastomeric systems are obvious choices for such applications, they could also be

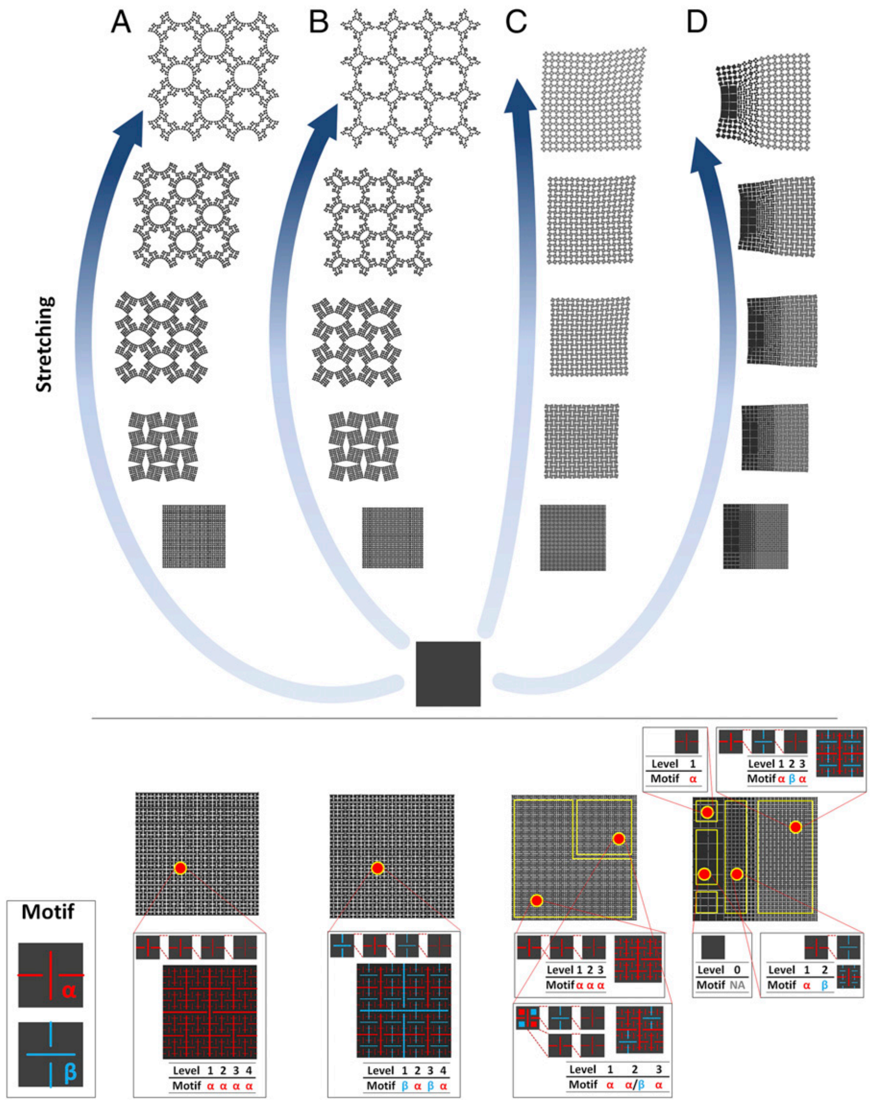

Fig. 2. Two cut motifs in a hierarchical structure. The cuts shown in red (blue) refer to the α-motif (β-motif). The β-motif is a 90° rotation of the α-motif in two dimensions. (*A*) The pure α-motif has a maximum lateral strain of 108% at level 4, ε_4(αααα). (*B*) The alternating α- and β-motif at level 4, ε_4(βαβα), yields a maximum lateral strain of 130%. (*C*) Inhomogeneous deformation can be realized by varying the α- and β-motif in a level-3 structure or (*D*) by mixing regions of different cut levels as indicated at the bottom of the figure. These examples were determined from finite element calculations with material parameters for silicone rubber.

fabricated from metals provided h/w is sufficiently small to limit the stresses in the hinge to be below the yield strength.

Fractal Cut Pattern: Motif

Besides hierarchy, another design parameter is the cut motif. In the previous section, the cut motif was constant (square or triangular), as indicated by the red lines in Fig. 1*B* (the α-motif). This same motif applied homogeneously leads to the same unit rotation pattern across the entire structure (white and yellow arrows in Fig. 1*A*). The number of degrees of freedom F grows monotonically with the hierarchy level N, whereas the increment of rotation angle becomes smaller. For example, the rotation angle of the smallest unit in the level-1 structure in Fig.1*B* is 45°, but the rotation angle for the smallest units in the level-2 structure is ~27°, ~12° for the smallest unit in the level-3 structure, and ~8° for the level-4 structure in Fig. 2*A* (see *Supporting Information* for details). This implies a finite limit to the expandability of structures with identical motifs.

Another motif, β, can be formed by rotating the α-motif by 90°, as shown in blue at the bottom of Fig. 2. In this motif the square units rotate in opposite directions relative to those in the α-motif. The combination of α- and β-motif between levels, hence, produces alternating rotation directions of the units, leading to larger rotation angles and strains at higher levels. We denote the strain at each level i in an N-level structure as $\varepsilon_N(x_1 x_2 \ldots x_N)$, where x_i denotes the motif (e.g., x_i refers to the α- or β-motif). For example, the maximum lateral strain in the level-4 structure consisting of a single cut motif is ε_4(αααα) = ε_4(ββββ) = 108% (Fig. 2*A*), whereas for the alternating motif it is ε_4(βαβα) = 130% (Fig. 2*B*).

Engineering Shape and Structure via Fractal Cut

Hierarchical levels and motifs provide the basic palette that can be used to draw (i.e., cut pattern) on a blank canvas (or material sheet). Different motifs and levels give different rotation patterns and strains, allowing for tunability. For the case of two motifs, we can evaluate the total number of ways

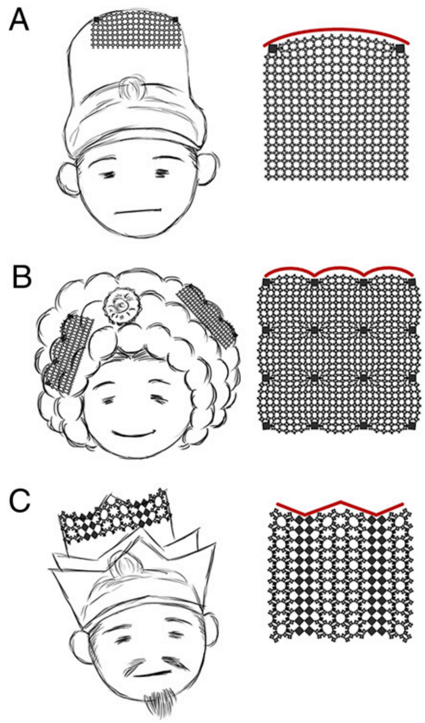

Fig. 3. Fractal cut Korean traditional hat and hairstyle realized by engineering the distribution of hierarchy and motif. (*A*) A *Tangon* hat from combination of $2 \bullet \varepsilon_0 + 68 \bullet \varepsilon_3(\alpha\beta\alpha) + 11 \bullet \varepsilon_4(\beta\alpha\beta\alpha)$ units, (*B*) a *Gache* hairstyle from a combination of $16 \bullet \varepsilon_0 + 132 \bullet \varepsilon_3(\alpha\beta\alpha) + 21 \bullet \varepsilon_4(\beta\alpha\beta\alpha)$, and (*C*) a *Jeongjaguan* hat from a combination of $12 \bullet \varepsilon_1(\alpha) + 24 \bullet \varepsilon_4(\beta\alpha\beta\alpha)$ as determined from finite element calculations with material parameters for silicone rubber.

to cut the material. At the first level, where the α- or β-motif can be applied, there are only two permutations, i.e., $V_1 = 2$. At level 2, each of the four subsquares has one of two motifs (i.e., 2^4 possibilities). Therefore, in a level-2 structure, $V_2 = 2^4 \times 2 = 32$. More generally, a level N structure with two motifs has

$$V_N = 2^{\sum_{n=1}^{N} 4^{n-1}} = \prod_{n=1}^{N} 2^{4^{n-1}} = 2^{\left(\frac{4^N-1}{3}\right)}. \qquad [1]$$

Here, level and motif distributions represent a mechanism for pluripotency. The original sheet (intact square) is pluripotent; when the fractal cut design is embedded, the sheet becomes unipotent. Upon stretching, the rotation of the units activates the differentiation. The final sheet shape can be programmed. For example, Fig. 2*C* shows the nonuniform expansion of a level-3 structure with an inhomogeneous combination of α- and β-motifs, and Fig. 2*D* shows the expanded shape resulting from a mixture of different hierarchy levels and motifs. We can exploit the pluripotency of a single square sheet to reproduce shapes of considerable complexity. Fig. 3 applies such an approach to reproduce traditional Korean hats and hairstyle.

Experimental Realizations

Structural differentiation was experimentally realized as shown in Fig. 4 *A*–*D*. We fabricated square sheets of silicone rubber with four different fractal cut patterns using three-dimensional printed molds. Fig. 4 *A*–*D* correspond to the simulated patterns from Fig. 2 *A*–*D*. By stretching, the square sheets show final shapes that very nearly match the simulation results. Obviously, the concept of fractal cut is not confined to a specific material system or to a specific feature size. For example, reducing the smallest feature scale in the level-4 structures in Fig. 4 *A* and *B* from 2 mm to 40 μm using photolithography to make molds into which polydimethylsiloxane (PDMS) sheets were cast leads to identical differentiation (see Fig. 5 and the *Supporting Information* for more experimental details). Hence, the present approach to forming highly expandable pluripotent materials can be applied on the macro- or microscale.

Discussion

Our pluripotent material approach provides an effective means for the design of structural platforms for stretchable and flexible devices.

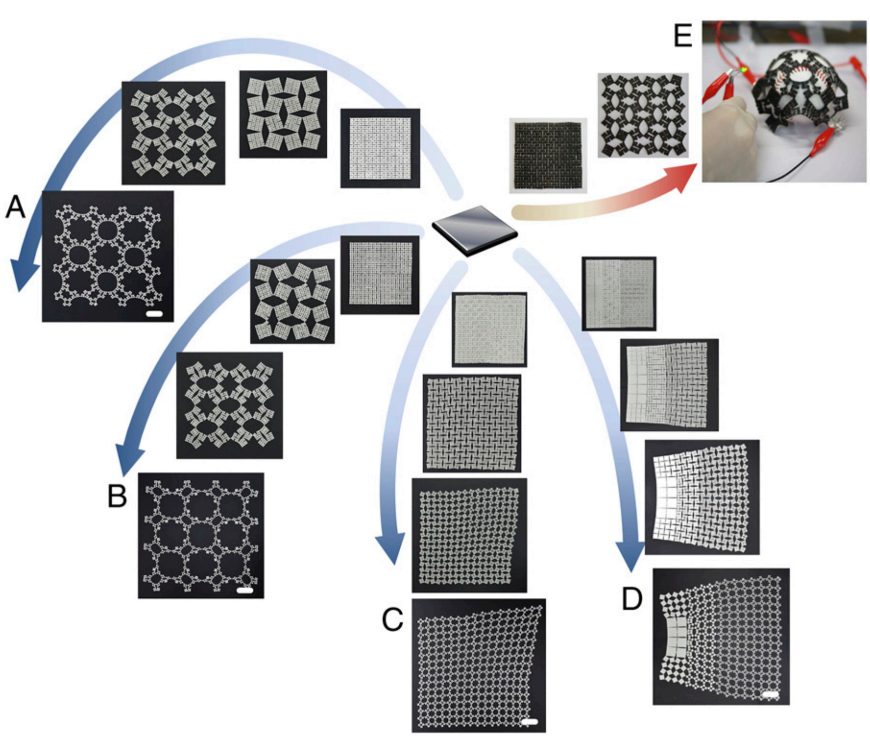

Fig. 4. Macroscopic experimental realization. Silicone rubber sheets differentiated with patterned cuts identical to those used in the finite element calculations. The smallest feature size (hinge width) is 2 mm. *A*–*D* correspond to the cut patterns in Fig. 2 *A*–*D* (these samples were pinned open to show expanded states). The correspondence between simulation and experiment is excellent. (*E*) A proof of concept for a stretchable electrode platform is shown by embedding $\varepsilon_3(\alpha\alpha\alpha)$ fractal cuts in a silicone rubber sheet coated with a thin conducting film and conformably wrapping the structure around a spherical baseball without wrinkles. The green LED light remains lit after wrapping. (The white lines in the expanded structure images are 40 mm.)

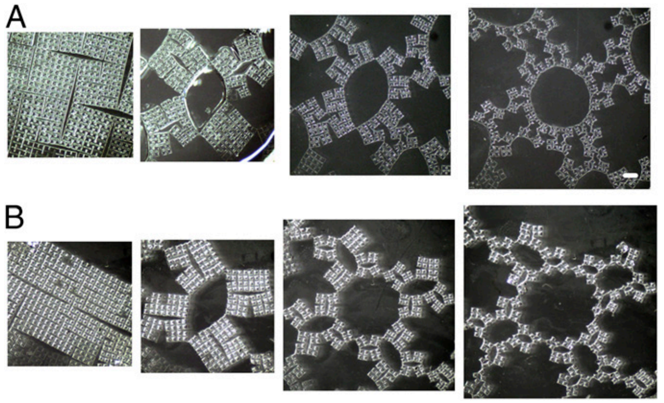

Fig. 5. Microscopic experimental realization. PDMS sheets differentiated with patterned cuts. The smallest feature size (hinge width) is 40 μm. (*A*) One unit of the homogeneous $\varepsilon_4(\alpha\alpha\alpha\alpha)$. (*B*) One unit of the $\varepsilon_4(\beta\alpha\beta\alpha)$. The correspondence between finite element simulation, macroscopic experiment, and microscopic experiment is excellent (cf. Figs. 2, 4, and 5). (The white line in the expanded structure image is 200 μm.)

Because stretching occurs by unit rotation rather than deformation, the material in the structure is inherently (nearly) strain-free (except at the hinge points); this is essential for stretchable platforms. It can also be strained without buckling. Thus, deformation of the structure will not alter the physical properties/function of the materials deposited on top of the units. Fig. 4*E* shows a proof of concept of a stretchable electrode with a fractal cut. We deposited a conductive film of multiwall carbon nanotubes on a silicone rubber sheet with an embedded homogeneous $n = 3$, α-motif. A light-emitting diode (LED) continues to be powered through the conductive film as the cut silicone rubber sheet is stretched over a spherical baseball (see *Supporting Information* for more experimental details). The conformal wrapping of the sheet around a nonzero Gauss curvature object (a sphere in this case) leads to nonuniform stretching (and nonuniform opening patterns), which can easily be accommodated by the fractal cut sheet (an example for other, nonbiaxial loads is shown in *Supporting Information*). Our approach to stretchable/flexible substrates differs from others in the literature, where expansion and conformal wrapping of a flexible device consisting of rigid components connected through stretchable elements (e.g., springs and serpentines) (15, 24, 25). In our systems, because the deformation is based on unit rotation we can fabricate a highly expandable device (e.g., ∼800% areal expansion from the level-6 (βαβαβα) structure; see *Supporting Information* for details) by placing conventional hard devices (e.g., battery, circuit, LED, etc.) on the rotating units without sacrificing device performance during large deformation.

Although an ideal fractal cut material expands by the rotation of rigid units meeting at free hinges, this is only an idealization. Our experimental realizations, however, are made with cuts that leave a finite ligament between the units. This has two consequences: First, these ligaments are strained and, second, this provides a small resistance to rotation (i.e., the hinges are not completely free). Nonetheless, a comparison of the experimental realization, its finite element simulation, and the rigid-unit/free-hinge model are in excellent correspondence (see *Supporting Information* for details). This implies that the theoretical idealization is not unreasonable and the approach can be applied to any material where hinge-like structures are possible; here, for simplicity the concept was demonstrated with silicone rubber and PDMS. Material design to achieve target expandability distributions/morphologies is an inverse problem in cut geometry. Unlike many materials design problems, the inverse problem for fractal cut structures is relatively straightforward with the simple design palette (cuts) described here and the straightforward calculations implied by the theoretical idealization.

Although the present results focused on two-dimensional sheets with square-based units as a starting point, the same approaches can be applied with (*i*) a different two-dimensional base unit [see *Supporting Information* for a triangular (kagome) lattice example] and (*ii*) three-dimensional materials using one of the many recent technological advances in three-dimensional printing (see *Supporting Information* for a free-hinge numerical example based on rotating cubes). By prescribing the geometry of cuts in a sheet we can simply control not only the meso/nano structure of a sheet but also engineer all of the properties that map to its structure, including those associated with shape (pore size, pore shape, macrogeometry, and maximum strain), mechanical properties (full stiffness tensor), and even material properties coupled with structures (electrical, photonic, and acoustic properties). Many of these require additional manipulation of the connections between the rotating units (e.g., stiffness depends on finite length of the material in hinges). Designing actuation or prerotations into the structure can further enhance the flexibility and functionality of cut structures for various applications.

ACKNOWLEDGMENTS. Y.C. and I.-S.C. thank Y. Kim and K. Lee for comments and support. This research was mainly supported by the Korea Institute of Science and Technology Internal Research Funding (Grants 2Z04050 and 2V03320) and National Research Council of Science and Technology (NST) Grant NST-Yunghap-13-1. Y.C. acknowledges support from the Research Fellowship for Young Scientists Program of Korea Research Council of Fundamental Science and Technology. Y.C. and S.Y. acknowledge partial support from National Science Foundation (NSF)/Emerging Frontiers in Research and Innovation (EFRI)–Science in Energy and Environmental Design (SEED) Award EFRI-1038215 and NSF/Origami Design for Integration of Self-Assembling Systems for Engineering Innovation (ODISSEI) Award EFRI-1331583. J.L. acknowledges support from NSF/Chemical, Bioengineering, Environmental, and Transport Systems (CBET) Grant 1240696 and Division of Materials Research (DMR) Grant 1120901. S.Y. and D.J.S. acknowledge partial support from NSF/Materials Research Science and Engineering Center (MRSEC) Award to University of Pennsylvania, DMR Grant 1120901. H.N.H. was supported by the Basic Science Research Program through the National Research Foundation of Korea funded by the Ministry of Science, Information and Communications Technology and Future Planning Grant 2013008806.

1. Babaee S, et al. (2013) 3D soft metamaterials with negative Poisson's ratio. *Adv Mater* 25(36):5044–5049.
2. Bauer J, Hengsbach S, Tesari I, Schwaiger R, Kraft O (2014) High-strength cellular ceramic composites with 3D microarchitecture. *Proc Natl Acad Sci USA* 111(7): 2453–2458.
3. Bertoldi K, Reis PM, Willshaw S, Mullin T (2010) Negative Poisson's ratio behavior induced by an elastic instability. *Adv Mater* 22(3):361–366.
4. Grima JN, Alderson A, Evans KE (2004) Negative Poisson's ratios from rotating rectangles. *Comp Methods Sci Technol* 10(2):137–145.
5. Grima JN, Evans KE (2000) Auxetic behavior from rotating squares. *J Mater Sci Lett* 19:1563–1565.
6. Kane CL, Lubensky TC (2014) Topological boundary modes in isostatic lattices. *Nat Phys* 10(1):39–45.
7. Kang SH, et al. (2014) Complex ordered patterns in mechanical instability induced geometrically frustrated triangular cellular structures. *Phys Rev Lett* 112(9):098701.
8. Kang SH, et al. (2013) Buckling-induced reversible symmetry breaking and amplification of chirality using supported cellular structures. *Adv Mater* 25(24):3380–3385.
9. Mosadegh B, et al. (2014) Pneumatic networks for soft robotics that actuate rapidly. *Adv Funct Mater* 24(15):2163–2170.
10. Overvelde JTB, Shan S, Bertoldi K (2012) Compaction through buckling in 2D periodic, soft and porous structures: Effect of pore shape. *Adv Mater* 24(17):2337–2342.
11. Schenk M, Guest SD (2013) Geometry of Miura-folded metamaterials. *Proc Natl Acad Sci USA* 110(9):3276–3281.
12. Shan S, et al. (2014) Harnessing multiple folding mechanisms in soft periodic structures for tunable control of elastic waves. *Adv Funct Mater* 24(31):4935–4942.
13. Sun K, Souslov A, Mao X, Lubensky TC (2012) Surface phonons, elastic response, and conformal invariance in twisted kagome lattices. *Proc Natl Acad Sci USA* 109(31): 12369–12374.
14. Taylor M, et al. (2014) Low porosity metallic periodic structures with negative Poisson's ratio. *Adv Mater* 26(15):2365–2370.
15. Webb RC, et al. (2013) Ultrathin conformal devices for precise and continuous thermal characterization of human skin. *Nat Mater* 12:938–944.
16. Bückmann T, et al. (2014) On three-dimensional dilational elastic metamaterials. *New J Phys* 16:033032.

17. Blees M, Rose P, Barnard A, Roberts S, McEuen PL (2014) Graphene kirigami. *Bulletin of the American Physical Society* 59(1):L30.00011 (abstr). Available at meetings.aps.org/link/BAPS.2014.MAR.L30.11. Accessed November 12, 2014.
18. Liu Y, Boyles JK, Genzer J, Dickey MD (2012) Self-folding of polymer sheets using local light absorption. *Soft Matter* 8(6):1764–1769.
19. Silverberg JL, et al. (2014) Applied origami. Using origami design principles to fold reprogrammable mechanical metamaterials. *Science* 345(6197):647–650.
20. Mandelbrot BB (1983) *The Fractal Geometry of Nature* (Freeman, New York).
21. Slack JMW (2008) Origin of stem cells in organogenesis. *Science* 322(5907):1498–1501.
22. Fan JA, et al. (2014) Fractal design concepts for stretchable electronics. *Nat Commun* 5:3266.
23. Synge JL, Griffith BA (1949) *Principles of Mechanics* (McGraw-Hill, New York).
24. Rogers JA, Someya T, Huang Y (2010) Materials and mechanics for stretchable electronics. *Science* 327(5973):1603–1607.
25. Suo ZG (2012) Mechanics of stretchable electronics and soft machines. *MRS Bull* 37(3):218–225.

Supporting Information

Cho et al. 10.1073/pnas.1417276111

SI Theoretical and Experimental Methods

To verify and realize the fractal design concepts presented in the manuscript, we performed a series of calculations using an idealized geometric model with rigid units and free hinges, a series of calculations using finite element simulations based on finite hinge width and realistic mechanical properties of a flexible material, and corresponding experiments with flexible materials with cut patterns identical to those in the finite element simulations. The details of the theoretical/numerical calculations and experimental work are presented below.

Geometric Model and Analytical Predictions. The geometric model is built on the assumption that all of the 2D units are rigid and that they are connected via freely rotating hinges. Consider first the case of the square-based fractal cut geometry of Fig. 1. The lateral strains of the level-1 structure can be expressed as

$$\varepsilon = \cos\theta + \sin\theta, \tag{S1}$$

where ε is the lateral strain and the angle θ is defined in Fig. S1*A*. This angle is the single degree of freedom in the level-1 structure. The maximum lateral strain for this structure (Fig. S1*B*) is

$$\theta^* = \pi/4 \tag{S2}$$

$$\varepsilon^* = \sqrt{2} - 1 \approx 0.41. \tag{S3}$$

The lateral strain of the level-2 structure can be expressed as

$$\varepsilon_x = \cos\theta_1 + ½\sin\theta_1 + ½\cos\theta_2 - 1 \tag{S4}$$

$$\varepsilon_y = \cos\theta_2 + ½\sin\theta_2 + ½\cos\theta_1 - 1, \tag{S5}$$

where the angles θ_1 and θ_2 are defined in Fig. S1*C*. These angles constitute the only two degrees of freedom of this structure. The maximum lateral strains in this structure (Fig. S1*D*) are

$$\theta_1^* = \theta_2^* = \arctan(½) \tag{S6}$$

$$\varepsilon_x^* = \varepsilon_y^* = 7/\left(2\sqrt{5}\right) - 1 \approx 0.565. \tag{S7}$$

The constraints on the angles are linear at level 2 but become nonlinear for higher levels. The constraints prevent interpenetration of the rigid, square units. For level 2, these constraints are

$$0 \le \theta_1 \le \pi/2 \tag{S8}$$

$$0 \le \theta_1 + \theta_2 \le \pi/2. \tag{S9}$$

Fig. S2 shows the allowable angles and lateral strains in the level-2 structure.

To simulate the opening of the fractal cut structures within the rigid unit/free hinge model, we implemented the geometric model within the Bullet Physics Library (1), a physics engine for simulation of rigid and soft body dynamics and collision detection. Static equilibrium structures were determined by damping the dynamics. Dynamics (Newtonian) were modeled by assigning a mass density to the material. The underlying model was also extended by applying a finite rotational stiffness to the otherwise free hinges.

Finite Element Simulation. The finite element simulations were performed using the implicit finite element software ABAQUS/Standard (2). A finite hinge width/thickness (w/h = 1, Fig. 1*C*) was adopted for comparison with the experiments. The edge length of the smallest square unit in all simulations was set to L = 8 mm and the hinge thickness and width were $h = w = 2$ mm. For all finite element simulations the ratio L/w = 4 was used. The material was linear elastic with properties chosen to match silicone rubber (Young's modulus = 2 MPa, Poisson's ratio = 0.49). Geometrical nonlinearity was considered under the plane strain constraint. The two-dimensional continuum element, CPE4, was adopted with the characteristic element length in the 0.25- to 0.5-mm range. We consider the calculation converged when the average force for all nodes is less than a predefined tolerance (0.5% of the largest force). The model was defined to be in moment equilibrium where a small increase in the strain led to a sudden increase in the nodal forces—this corresponds to the onset of deformation of one or more material units (rather than primarily rotation of units).

Experimental Methods. We experimentally demonstrated the expansion of the fractal cut pattern in both large-scale (macroscopic) and small-scale (microscopic) samples. All of the experimental samples have the same geometry ratios as in the finite element model (L/w = 4).

Macroscopic sample preparation. The macroscopic experiments were performed on materials fabricated by using a three-dimension printer (Objet260 Connex; Stratasys) to print a hard, patterned mold into which silicon rubber was cast to form a patterned membrane. Commercial silicone rubber (SILASTIC 3481 Base and SILASTIC 81 Curing Agents; Dow Corning) was used as the membrane material. All of the experiments were performed at room temperature. We used pins to fix the stretched membrane at finite strain in Fig. 4.

Microscopic sample preparation. The microscopic samples were formed as follows. A patterned mold of SU-8 was created via photolithography. PDMS was cast into the mold to form a replicate membrane. The thickness of membrane was 80–100 μm. The membrane was released from the mold and placed onto a glass sheet, to which it adhered. The sheets were released from the substrate by the addition of ethanol and stretched at room temperature. When the ethanol evaporated the membrane adhered to the substrate in its open configuration. Adding and evaporating ethanol led to reversible adhesion and release.

Comparison of the Geometrical Model, the Finite Element Calculations, and the Experiments. Fig. S3 shows level-3 (ααα) structures stretched to their maximum biaxial strain as determined using the geometrical (rigid unit/free hinge) model (Fig. S3*A*), the finite element calculation (Fig. S3*B*), and the experimental macroscopic silicone rubber sample (Fig. S3*C*). Excellent correspondence between all three realizations of the level-3 (ααα) structure is obtained. The same level of agreement between the simulation and experiment was shown by comparison of Figs. 2 and 4 in the main text.

SI Characteristics of Mechanical Deformation

Moment Equilibrium: Biaxial Loading. To demonstrate the expandability of the hierarchical structure for a larger number of levels than shown in the text we performed finite element calculations for the level-6 (βαβαβα) case at its maximum lateral strain (Fig. S4). The maximum biaxial strain was $\varepsilon^* \sim 1.8$, such that the area expanded by $(1 + \varepsilon^*)^2$ or ∼800%. Although the overall areal expansion is large, no hinge rotates (bends) by an angle of more than 45° and most exhibit much smaller opening angles. In the most extreme case, the maximum 45° opening in the level-1 structure, less than 1% of the material reaches a true strain of 0.3 true strain (localized in a small section of the hinge material).

Uniaxial Loading. For level-1 square cut patterns, there is only one degree of freedom. Hence, the biaxial and uniaxial load case will lead to identical expanded structures. However, for levels >1, the uniaxially stretched configurations differ from those observed under biaxial load. Fig. S4 shows the case of the uniaxial (stress) deformation of a level-3 (ααα) silicone rubber sample (with 4 × 4 repeat units) as determined from the finite element calculations (as in the results presented earlier, the edge length of the smallest square unit was $L = 8$ mm and the hinge dimensions were $h = w =$ 2 mm). Auxetic behavior was clearly observed to uniaxial displacements up to ∼300 mm; the calculated Poisson's ratio was negative. It should also be noted that at larger displacements (post moment equilibrium) the structure showed conventional deformation with a positive Poisson's ratio. In these finite element calculations the square units were prevented from overlapping.

Nonsquare Rotating Units (Two-Dimensional Kagome and Three-Dimensional Cube). Although the text focuses primarily on two-dimensional, square-based fractal cuts, the fractal cut approach is not confined to this specific shape (square). In principle, any recursive cut patterns that divide a material into hierarchical rotating units can be used as the basis for these fractal cut materials. For example, triangular units making up a kagome structure (3, 4) is a good example of a nonsquare unit in two dimensions. Fig. S6 shows an example of such a level-2 kagome structure. The smallest unit in this structure is still triangular, and hence it can be divided into smaller triangles to make higher-level patterns. Movies S2 and S3 show the expansion of level-2 and -3 kagome structure under in-plane biaxial stretching. These images and movies were prepared using the Bullet Physics Library (1) in a rigid units/finite hinge stiffness model.

We also applied this approach to three-dimensional structures. Movies S4 and S5 show the balanced triaxial stretching of a level-1 and level-2 structure in three dimensions where the individual units are cubes with corner hinges. These calculations were also performed using the Bullet Physics Library (1).

Fig. S7 shows several examples of fractal cut and expanded structures in two dimensions and three dimensions to demonstrate that the concept of the fractal cut is not confined to the set of cases shown explicitly in the paper and is quite general.

Stretchable Electrodes and Conformal Wrapping.

Fabrication of stretchable electrode membrane. The fractal cut silicone rubber membranes shown in the text were converted to electrodes by coating with a conducting layer. The coating solution was prepared as follows. Single-wall carbon nanotubes, SWCNTs (ASP-100F; Hanhwa Nanotech) were ground with 1-butyl-3-methylimidazolium bis(trifluoromethylsulfonyl)imide (BMIM TFSI) (Sigma-Aldrich) to form gels. The SWCNT gels were dispersed in toluene for 1 h via bath sonication. Silicone rubber (KE-441; ShinEtsu) was added to the solution. This mixture was stirred for 3 h at room temperature. The SWCNT/BMIM TFSI/KE-441 solution was sprayed onto the silicon rubber level-3, square, fractal cut membrane and dried in a room-temperature vacuum oven for more than 1 d. The coated substrates were held in a saturated nitric acid vapor at 70 °C for 30 min to enhance their conductivity and then completely dried in a vacuum oven. Fig. S8 shows a lit green LED that was powered by a battery in series with this SWCNT-coated silicone rubber fractal cut membrane before (Fig. S8*A*) and after (Fig. S8*B*) stretching. Clearly, the LED remains illuminated up to the maximum strain (lateral strain of 43%).

Conformal wrapping. As shown in Fig. 4*E* the stretchable electrode using the patterned sheet can wrap around three-dimensional objects with surfaces of nonzero Gauss curvature. Fig. S8*C* shows an experimental example of the wrapping of the SWCNT-coated, fractal cut membrane around a (sphere) baseball without interrupting the LED circuit. We used the Bullet Physics Library (1) to simulate the expansion and wrinkle-free conformal wrapping of a nonzero Gauss curvature object (a sphere and a cube here) with homogeneous level-3 (ααα) structures (Fig. S9 and Movies S6 and S7). This demonstrates the high degree of conformability and nonuniform expandability of fractal cut membranes.

1. Bullet Physics Library. Available at bulletphysics.org. Accessed November 12, 2014.
2. ABAQUS/Standard. Available at www.3ds.com/products-services/simulia/portfolio/. Accessed November 12, 2014.
3. Kane CL, Lubensky TC (2014) Topological boundary modes in isostatic lattices. *Nat Phys* 10(1):39.
4. Sun K, Souslov A, Mao X, Lubensky TC (2012) Surface phonons, elastic response, and conformal invariance in twisted kagome lattices. *Proc Natl Acad Sci USA* 109(31): 12369–12374.

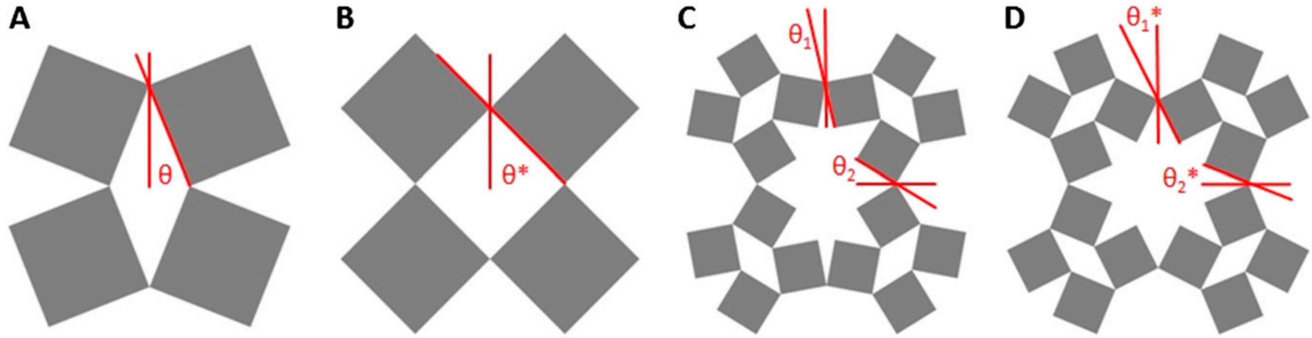

Fig. S1. Ideal geometry with rigid units and free hinges. Four rotating units in the level-1 structure at a (*A*) small strain and (*B*) at the maximum lateral strain. Sixteen rotating units in a level-2 structure corresponding to a (*C*) small biaxial strain and (*D*) at the maximum biaxial strain.

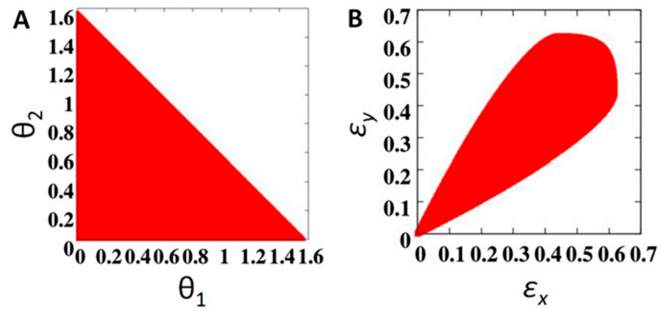

Fig. S2. Allowable hinge angles and strains in the level-2 structure. (*A*) The allowed angles θ_1 and θ_2 for the level-2 structure are shown in red. (*B*) The strains ε_x and ε_y that are realizable in the level-2 structure.

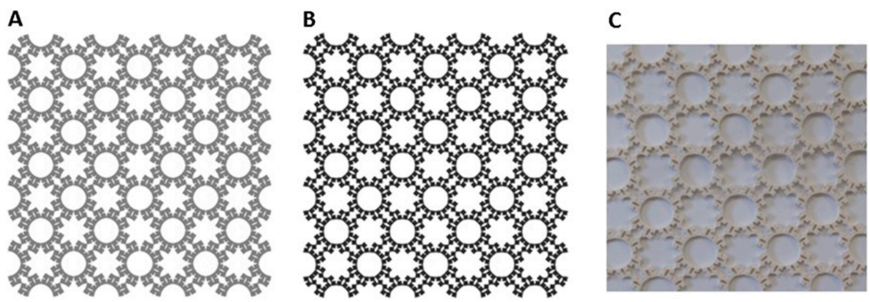

Fig. S3. Comparison of the geometrical model, finite element calculation, and experiment for a level-3 (ααα) structure at the maximum biaxial strain. A comparison of the biaxially stretched level-3 (ααα) structures obtained using (*A*) the geometrical (rigid unit and free hinge) model (1), (*B*) the finite element calculation (2) for a hinge of $h = w = L/4$ (L is the length of the edge of the smallest square unit; Fig. 1*C*), and (*C*) the silicone rubber sample (exactly the same hinge geometry as in *B*).

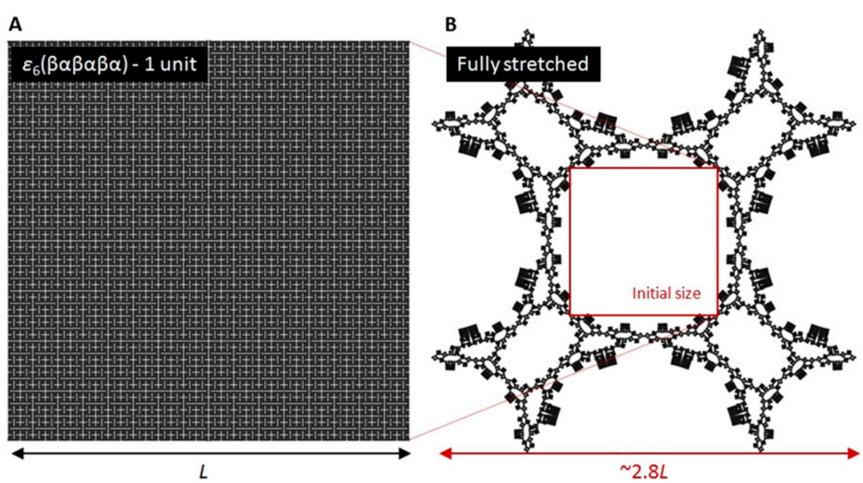

Fig. S4. (*A*) The level-6 (βαβαβα) structure at the maximum biaxial strain obtained using the finite element method. (*B*) The initial (unstretched) sample size.

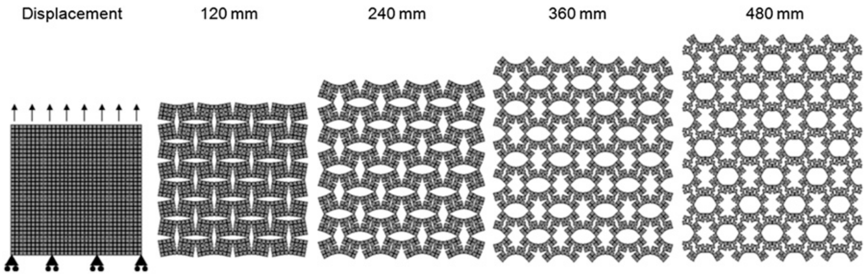

Fig. S5. Uniaxial loading. Uniaxial (stress) deformation of a level-3 (ααα) 4 × 4 unit structure at different displacements as determined using the finite element calculations. The edge length of the smallest square unit in the structure was 8 mm, and the hinge width was 2 mm. Auxetic behavior is clearly observed for uniaxial displacements up to ∼300 mm. Below this strain, the structure deforms effectively via "free hinge" rotation, and above this strain the deformation occurs by stretching the material (rather than by rotation) in a more conventional fashion with a positive Poisson's ratio. The calculations do not allow interpenetration of the square units.

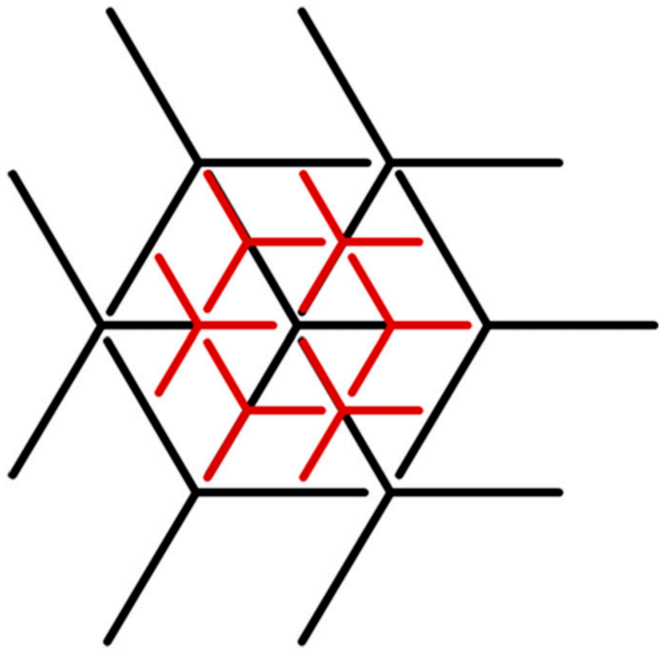

Fig. S6. Triangular (kagome) pattern. Black lines represent a level - kagome pattern breaking the material into six rotating triangular units. Red lines represent a level-2 kagome pattern. Similar to the square units in which different motifs may be obtained by a 90° rotation of the cut pattern, a different motif of the kagome pattern can be obtained by 60° rotation of the original cut pattern.

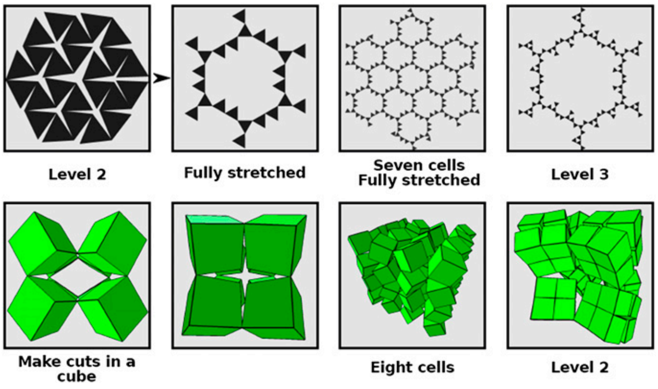

Fig. S7. Nonsquare units. The first row shows level-2 and level-3 expansions of (two-dimensional) kagome structures. The second row demonstrates level-1 and level-2 expansion of three-dimensional cubic units with corner hinges. These calculations were performed using the open source Bullet Physics software (1) (with an arbitrary rotational spring constant) (see also Movies S2–S5).

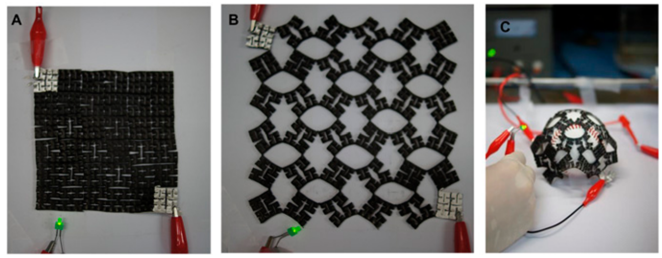

Fig. S8. Stretchable electrode on a silicone rubber substrate with a level-3 fractal cut pattern. (*A*) A green LED connected to a battery through a series circuit including the fractal cut electrode before stretching. (*B*) The LED light continues to be powered thorough the stretchable electrodes as the substrate is stretched to ∼43% lateral strain and (*C*) wrapped over the baseball (a nonzero Gauss curvature shape).

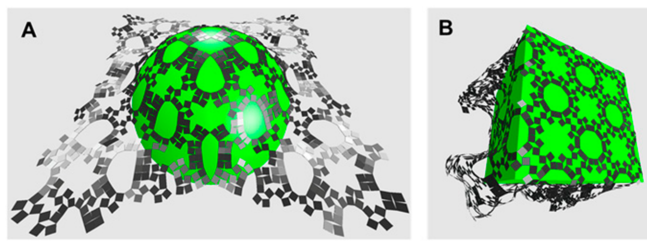

Fig. S9. Conformal wrapping of nonzero Gauss curvature object. A level-3 square unit fractal cut structure wrapped around (*A*) a sphere and (*B*) a cube. The calculations were performed using the rigid unit and angular hinge model via the open source Bullet Physics software (1) (with an arbitrary rotational spring constant). See Movies S6 and S7 for the draping dynamics.

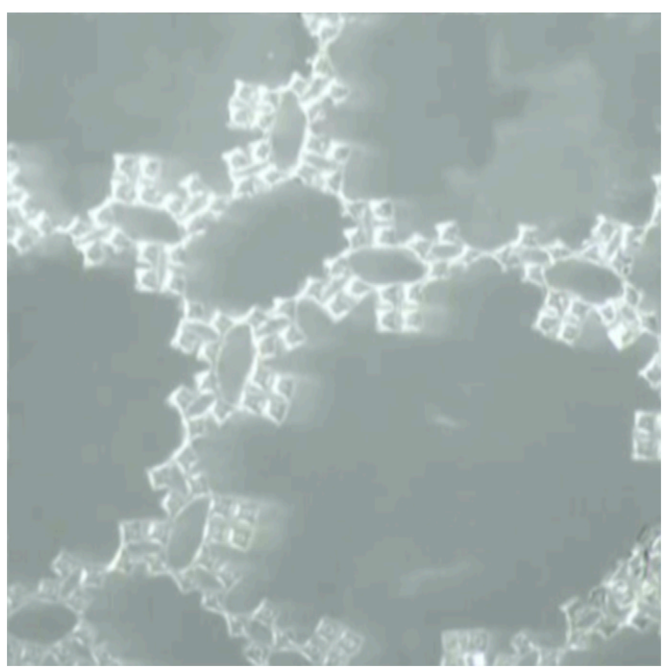

Movie S1. Releasing the stretched PDMS sheet. The stretched level 4 ($\beta\alpha\beta\alpha$) being released from the glass substrate by the addition of ethanol.

Movie S1

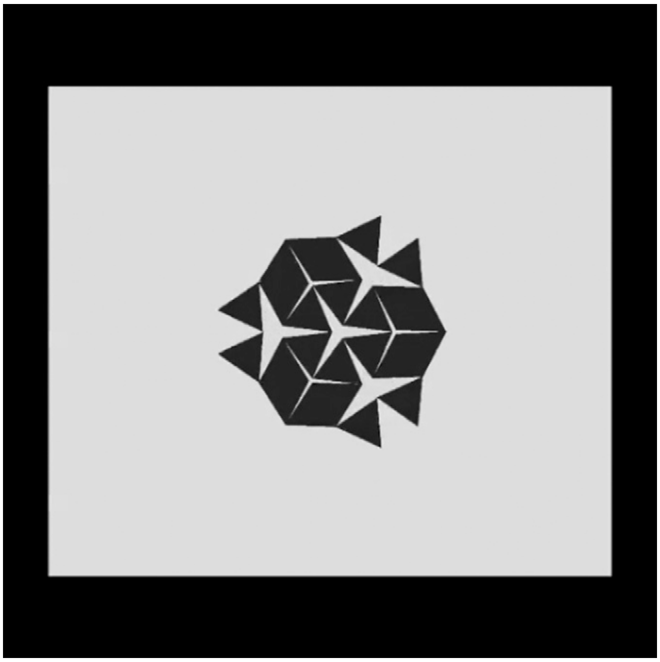

Movie S2. Stretching of the level-2 kagome structure.

Movie S2

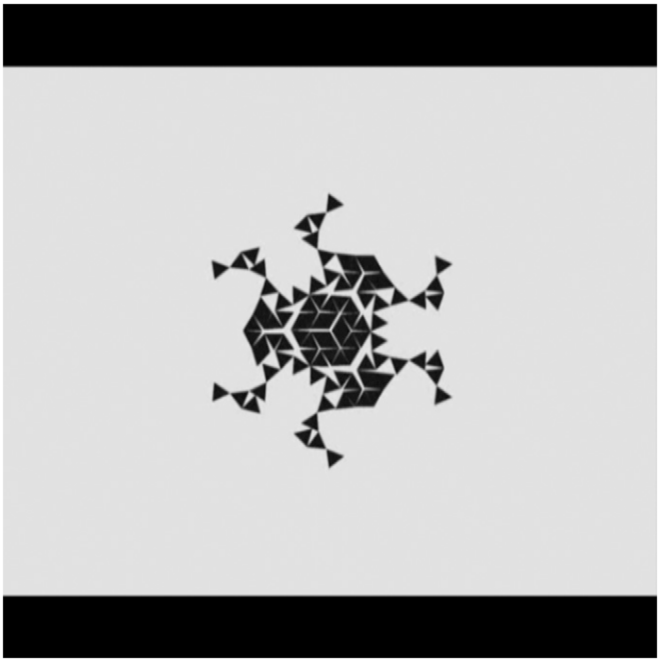

Movie S3. Stretching of the level-3 kagome structure.

Movie S3

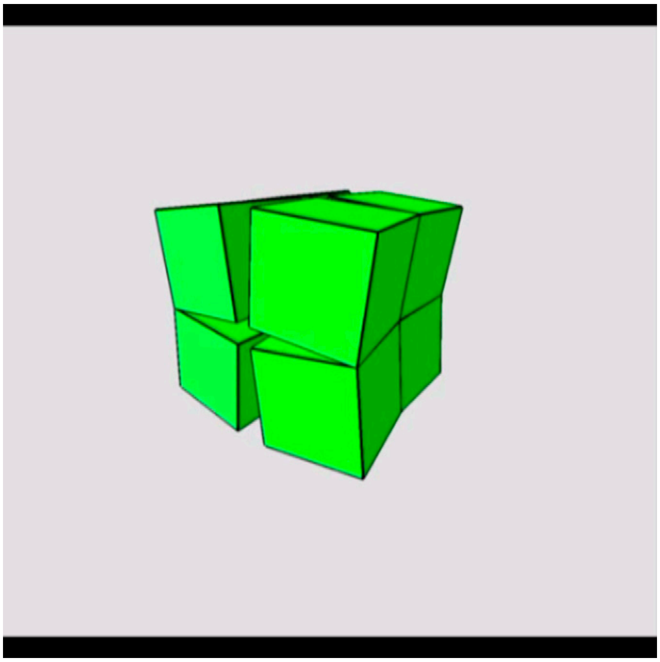

Movie S4. Stretching of the level-1 three-dimensional cubic structure [using the rigid unit, finite stiffness corner hinge model in Bullet Physics (1)].

Movie S4

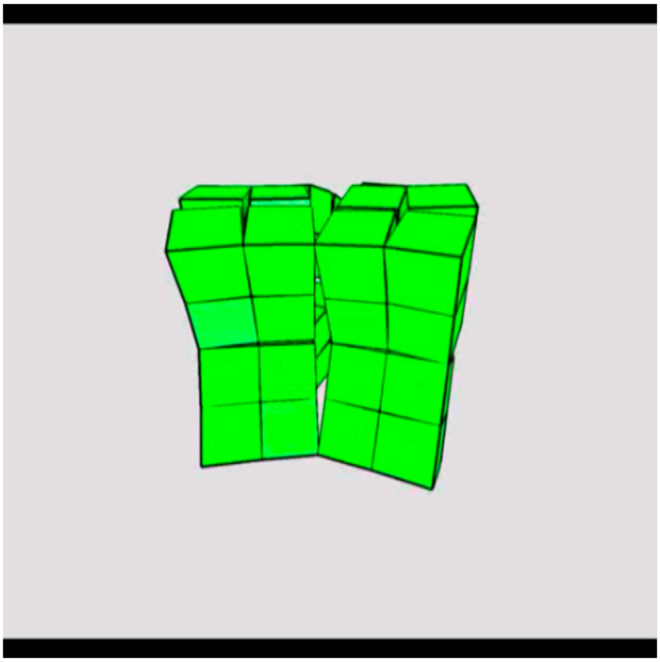

Movie S5. Stretching of the level-2 three-dimensional cubic structure [using the rigid unit, finite stiffness corner hinge model in Bullet Physics (1)].

Movie S5

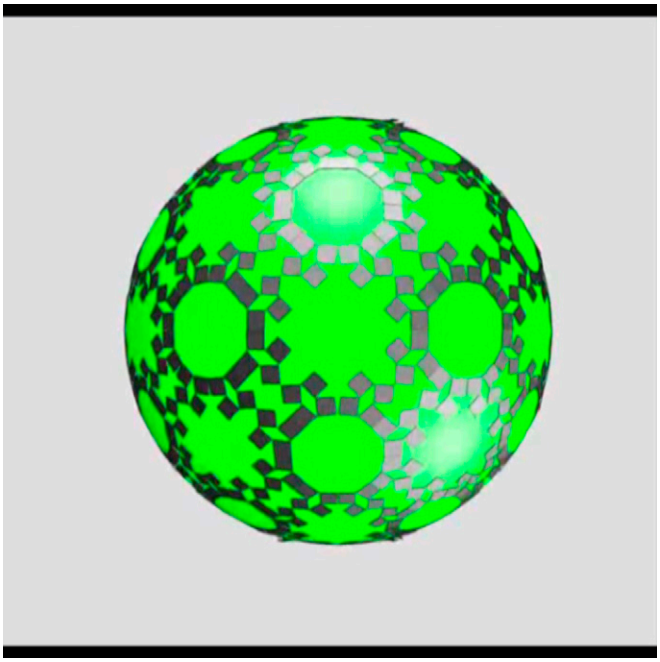

Movie S6. Conformal draping of a sphere by a two-dimensional fractal cut material with level-3 fractal cut structure [using the rigid unit, finite stiffness hinge model in Bullet Physics (1)].

Movie S6

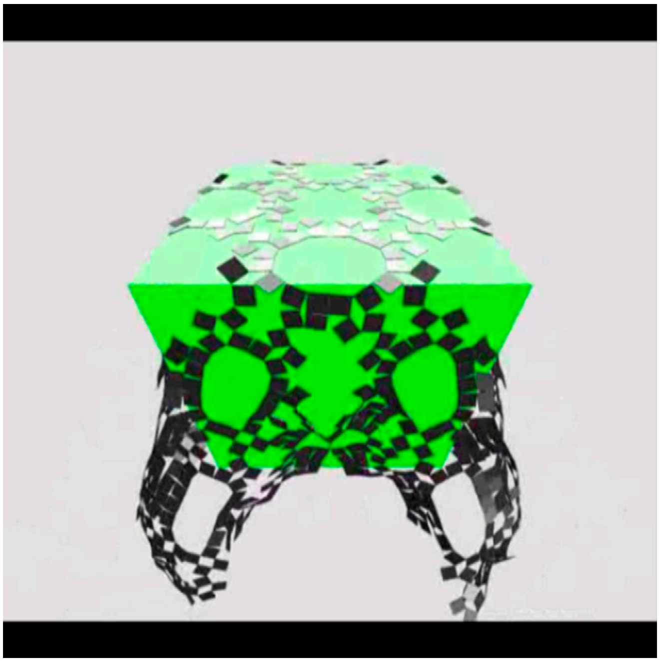

Movie S7. Conformal draping of a cube by a two-dimensional fractal cut material with level-3 fractal cut structure [using the rigid unit, finite stiffness hinge model in Bullet Physics (1)].

Movie S7